Electronic Transactions on Numerical Analysis.
Volume 61, pp. 105–120, 2024.

ISSN 1068–9613.
DOI: 10.1553/etna_vol61s105

ETNA
Kent State University and
Johann Radon Institute (RICAM)

A TWO-DIMENSIONAL INTEGRAL MODEL OF THE FIRST-KIND FOR LIN ELECTROMAGNETIC DATA INVERSION*

PATRICIA DÍAZ DE ALBA† AND FEDERICA PES‡

Dedicated to Professor Giuseppe Rodriguez on the occasion of his 60th birthday.

Abstract. In this paper we introduce a two-dimensional first-kind integral model to describe the interaction between the soil and an electromagnetic device. This model is used to reconstruct the electrical conductivity of the soil from electromagnetic data. The definition of the two-dimensional model is derived, and a numerical study of the forward model based on Gauss–Legendre quadrature formulae is presented. To solve the inverse problem, a linear system obtained from the discretization of the integral equation in the model is considered. The main difficulty is the severe ill-conditioning of the system, so the Tikhonov regularization method is applied and different regularization matrices and choice-rules for the regularization parameter are proposed. Several numerical tests show the effectiveness of the proposed approach.

Key words. first-kind integral equations, Gauss–Legendre quadrature, Tikhonov regularization, electromagnetic data

AMS subject classifications. 65R20, 65D32, 65Z05, 65F22

1. Introduction.

Electromagnetic induction (EMI) methods are common tools to investigate the conductivity and magnetic distributions of near-surface structures in a non-invasive way. The study and analysis of subsoil properties via electromagnetic techniques are relevant in various applications, e.g., for environmental and geotechnical investigations [25, 38] (including soil and water conservation [22, 32]), groundwater prospecting [37, 45], hydrological application in arid or semi-arid region [27, 44], precision agriculture [46], claypan soil properties [3, 47], mapping of soil salinity [33, 35, 48], and environmental quality [23].

A very common device used to measure electromagnetic data is the Ground Conductivity Meter (GCM). It is composed of a coil transmitter and a coil receiver placed at a fixed distance, ranging from 0.5m to around 6m. Nowadays, there exists multi-receiver GCM, making the problem larger and more difficult to solve. In this paper, we focus on single-receiver instruments. In 1980, McNeill [34] provided an important contribution to understand the principal properties of such devices, in particular of the Geonics EM31 and EM34 devices. More recently, the review [43] examined the role of the EM38 and EM38-MK2 devices in monitoring and mapping saline soils.

An alternating current, flowing into the transmitter, generates a primary magnetic field H_{P} into the subsurface. In the presence of conductivity variations in the subsurface, eddy currents are generated producing, in turn, a secondary magnetic field H_{S}. Finally, the ratio between both fields is recorded by the receiver. These devices can be used considering different orientations of the coils: horizontal, vertical, or perpendicular. The horizontal orientation of the coils corresponds to vertical magnetic dipoles (VMD), vertical coils are equivalent to horizontal magnetic dipoles (HMD), and perpendicular dipoles are denoted by PERP. Different depths can be reached depending on the configuration of the instrument: distance between the coils, operating frequency, and orientation.

*Received February 19, 2024. Accepted August 28, 2024. Published online on September 18, 2024. Recommended by M. Donatelli.

†Department of Mathematics, University of Salerno, via Giovanni Paolo II, 132, 84084 Fisciano, Italy (pdiazdealba@unisa.it).

‡Department of Mathematics and Computer Science, University of Cagliari, via Ospedale, 72, 09124 Cagliari, Italy (federica.pes@unica.it).

ETNA
Kent State University and
Johann Radon Institute (RICAM)

When one wants to investigate shallow targets at depths ranging up to several tens of meters, devices that make use of electromagnetic recordings at low induction number (LIN) are well suited. The induction number, denoted by B, is a constant which involves the instrument's scale and the scale of induced currents within the ground, and it is defined as the ratio between the inter-coil distance ρ and the skin depth δ of the currents in the ground, i.e.,

$$B = \frac{\rho}{\delta}, \qquad \delta = \sqrt{\frac{2}{\sigma\omega\mu_0}},$$

where σ is the electrical conductivity of the soil measured in Siemens per meter (S/m), ω is the angular frequency of the device computed as $2\pi f$, with f the frequency measured in Hertz (Hz), and $\mu_0 = 4\pi 10^{-7}$ Henries per meter (Hm^{-1}) is the magnetic permeability of free space [2]. We remark that B is a dimensionless quantity since both ρ and δ are measured in meters.

The GCM devices measure EM coupling ratios between the secondary electromagnetic field and the primary field. This is a complex number with in-phase (real part) and quadrature (imaginary part) components. The quadrature component is transformed into apparent conductivity by the formula

$$\sigma_a \approx \frac{4}{\omega\mu_0\rho^2}\,\mathfrak{Im}\left(\frac{H_{\mathrm{S}}}{H_{\mathrm{P}}}\right),$$

where $\mathfrak{Im}$ represents the imaginary part of the signal ratio. The in-phase part is in general very small in comparison to the quadrature component. A common assumption is that $B \ll 1$, which means that we are dealing with low conductivity values. In this way, a linear mathematical model can be applied to reconstruct accurately the electrical conductivity distribution.

However, other kinds of EM ground conductivity instruments exist and are typically multi-frequency devices with either fixed or variable coil separations. These devices are generally related to a high induction number B and require more complex modeling, i.e., nonlinear models. In the last few years, a nonlinear one-dimensional electromagnetic model has been studied in different situations and has been coupled with specific techniques for evaluating the Jacobian, useful to invert measurement datasets by the Gauss–Newton method regularized by truncated generalized singular value decomposition [28], together with automatic techniques for estimating the regularization parameter. In [16], the reconstruction of the electrical conductivity of the soil, assuming known magnetic permeability, considering only the quadrature component of the measurements was proposed. In [21], the latter algorithm was adapted to devices that allow for different configurations and can take multiple simultaneous measurements. In this work, the authors also considered the possibility of processing the in-phase component of the signal. The algorithm was updated to invert the whole complex signal sensed by the device, and in [14, 15] it was applied to invert datasets collected in Sardinia (Italy), at the Molentargius Saline Regional Nature Park. The paper [13] focuses on the identification of the magnetic permeability distribution under the assumption that the electrical conductivity is known beforehand. An important result of this work was to give an analytical expression of the Jacobian with respect to the variation of the magnetic permeability. A Matlab toolbox for the forward and the inverse procedures has been made publicly available in [11, 12]. This software was then used in [4] to obtain a two-dimensional reconstruction of the electrical conductivity of a vertical section of the soil by solving a variational problem as well as in [5], where an Alternating Direction Multiplier Method was applied. Finally, in [42], a minimal-norm regularized solution method based on the Gauss–Newton iteration to invert FDEM data is proposed, while in [6] an efficient implementation of the Gauss–Newton method

ETNA
Kent State University and
Johann Radon Institute (RICAM)

via generalized Krylov subspaces has been developed. We remark that in the papers cited above, the nonlinear model is one-dimensional, also in case of two-dimensional reconstructions, which were obtained by juxtaposing one-dimensional approximate solutions. To the best of our knowledge, two- or three-dimensional nonlinear models have not yet been studied and analyzed in depth because they are computationally challenging as one needs to consider the variation of the soil properties in two or three spatial variables, making the problem extremely large.

In this paper, we focus on the case of measurements at low induction number and we analyze a two-dimensional linear model, that is derived from a three-dimensional electromagnetic one. Such a three-dimensional linear forward EM model that computes the apparent conductivity using integral equations has been developed in [36] starting from Maxwell's equations. Other contributions were given in [40, 41], where the three-dimensional integral equation is transformed into a linear system, considering a discretization of the ground into prismatic cells.

We show that, for deriving the two-dimensional model using vertical magnetic dipoles, the integration along the y-axis can be evaluated in terms of elliptic integrals. In other cases, such as when using horizontal magnetic dipoles, the kernel functions are very complicated, and numerical integration is required. Since the two integral equations of the model contain the same unknown, we will consider just vertical magnetic dipoles. The horizontal case will not be covered in this paper, and it will be a topic of future research.

The numerical approach proposed here for the forward problem is based on the numerical approximation of the integral appearing in the model to obtain the approximated EM data. To this end, we opt for a Gauss–Legendre quadrature rule, but other kinds of formulae can be applied; see, for example, [19]. After that, we focus on the inversion procedure. By a collocation method, we discretize our problem leading to a linear system of equations to be solved by minimizing the residual function, i.e., the difference between the reconstructed and the measured data. The main difficulty is the severe ill-posedness of the problem. This means that it either has no solution in the desired class, or admits infinitely many solutions, or is such that small errors in the data may lead to arbitrarily large errors in the solution. For this reason, the problem needs to be regularized. In this paper, we apply the well-known Tikhonov regularization which includes an additional term in the least-squares problem to introduce prior information about the solution. Different regularization matrices can be used. The L-curve method is applied to choose the regularization parameter. Moreover, we compare this choice of the parameter with the optimal one.

We remark that, from the same three-dimensional model, we can derive the one-dimensional model studied in [34] and analyzed in [20], in which the authors studied the problem in different function spaces and applied collocation methods to lead to a linear system of equations combined with regularization techniques. In [17, 18], a numerical method based on the Riesz representation theorem operating in a reproducing kernel Hilbert space to compute the minimal-norm solution in the presence of boundary constraints was proposed.

The structure of this paper is as follows. In Section 2, the derivation of the two-dimensional model from the three-dimensional model is presented. The study of the forward model by approximating the integral in the equation is shown in Section 3, while the numerical approach for solving the inverse problem is reported in Section 4. Finally, Section 5 presents several numerical tests on synthetic data which show the effectiveness of the whole procedure. The conclusions are summarized in Section 6.

2. Derivation of the two-dimensional electromagnetic model. As we said in the previous section, we focus on the horizontal orientation of the coils, that is, on the vertical magnetic dipole VMD. The three-dimensional EM-LIN model is a first-kind integral equation

ETNA
Kent State University and
Johann Radon Institute (RICAM)

defined as

$$g(\mathbf{r}_T, \mathbf{r}_R; h) = -\frac{16\pi\rho}{\omega\mu_0 m_z} \int_{\mathcal{V}} G_{Hz}(\mathbf{r}, \mathbf{r}_R; h) E_{Hz}(\mathbf{r}, \mathbf{r}_T; h) \sigma(\mathbf{r}) \, \mathrm{d}^3\mathbf{r}, \tag{2.1}$$

where g is the vector of the observed apparent conductivity (i.e., the data recorded by the device), $\mathbf{r} = [x, y, z]^T$ is the position vector in the subsurface, $\mathbf{r}_T = [x_T, y_T, z_T]^T$ and $\mathbf{r}_R = [x_R, y_R, z_R]^T$ are the position vectors of the transmitter and the receiver, respectively, ρ is the inter-coil distance, ω is the angular frequency of the device, and μ_0 is the magnetic permeability of the free space. Let us assume that the device is positioned at height h above the ground. Then, $h = z_T = z_R$. The magnetic momentum of the transmitter in the z-direction is represented by m_z, $\sigma(\mathbf{r})$ is the conductivity distribution of the subsurface at position $\mathbf{r}$, and $\mathcal{V}$ is the three-dimensional domain of $\sigma(\mathbf{r})$. The magnetic dyadic Green's function of the half-space is defined as

$$G_{Hz}(\mathbf{r}, \mathbf{r}_R; h) = \frac{1}{4\pi} \left[-\frac{y - y_R}{\|\mathbf{r} - \mathbf{r}_R\|^3} \vec{i} + \frac{x - x_R}{\|\mathbf{r} - \mathbf{r}_R\|^3} \vec{j} \right],$$

and the electric field function induced within the earth is computed by

$$E_{Hz}(\mathbf{r}, \mathbf{r}_T; h) = -\frac{\omega\mu_0 m_z}{4\pi} \left[-\frac{y - y_T}{\|\mathbf{r} - \mathbf{r}_T\|^3} \vec{i} + \frac{x - x_T}{\|\mathbf{r} - \mathbf{r}_T\|^3} \vec{j} \right],$$

where

$$\|\mathbf{r} - \mathbf{r}_n\| = \sqrt{(x - x_n)^2 + (y - y_n)^2 + (z + h)^2}, \qquad n = T, R,$$

and the unit vectors $\vec{i}$ and $\vec{j}$ represent the x- and y-directions. Throughout the paper, the symbol $\|\cdot\|$ stands for the Euclidean norm; h and ρ are measured in meters.

REMARK 2.1. Notice that the expressions for the electric field and the Green's function have the same geometrical dependence. This means that interchanging $\mathbf{r}_T$ and $\mathbf{r}_R$ does not change equation (2.1).

After some algebraic steps, the equation in (2.1) can be explicitly represented as

$$\begin{aligned} &g(x_T, y_T, x_R, y_R; h) \\ &= \frac{\rho}{\pi} \int_0^{+\infty} \int_{-\infty}^{+\infty} \int_{-\infty}^{+\infty} \frac{(x - x_T)(x - x_R) + (y - y_T)(y - y_R)}{\|\mathbf{r} - \mathbf{r}_T\|^3 \|\mathbf{r} - \mathbf{r}_R\|^3} \sigma(x, y, z) \, \mathrm{d}x \, \mathrm{d}y \, \mathrm{d}z. \end{aligned} \tag{2.2}$$

If we integrate the model (2.2) along the y-direction, we obtain the two-dimensional model corresponding to the VMD configuration that has been studied in [41].

Following [39], the structure of the two-dimensional model implies that the electrical conductivity does not vary along the y-direction; see Figure 2.1. For simplicity, we also assume $y_T = y_R = 0$. The integral equation of the two-dimensional model is

$$g(x_T, x_R; h) = \frac{\rho}{\pi} \int_0^{+\infty} \int_{-\infty}^{+\infty} k(x, z, x_T, x_R; h) \sigma(x, z) \, \mathrm{d}x \, \mathrm{d}z, \tag{2.3}$$

where $\rho = |x_T - x_R|$ and the two-dimensional kernel is obtained by integrating with respect to y the three-dimensional kernel appearing in (2.2), that is,

$$\begin{aligned} &k(x, z, x_T, x_R; h) \\ &\quad = \int_{-\infty}^{+\infty} \frac{(x - x_T)(x - x_R) + y^2}{[(x - x_T)^2 + y^2 + (z + h)^2]^{3/2} [(x - x_R)^2 + y^2 + (z + h)^2]^{3/2}} \, \mathrm{d}y. \end{aligned}$$

ETNA
Kent State University and
Johann Radon Institute (RICAM)

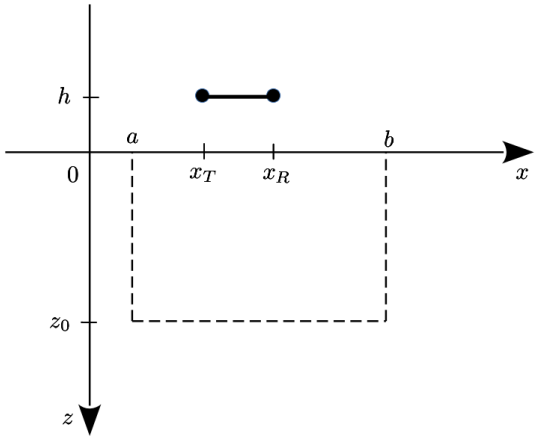

FIG. 2.1. *Representation of the two-dimensional model: the device moves along the x-direction when the y-direction is fixed. The vertical section of the subsoil of interest is the domain $[a, b] \times [0, z_0]$.*

Defining

$$c^2 := c^2(x, z, x_T; h) = (x - x_T)^2 + (z + h)^2, \tag{2.4}$$

$$p^2 := p^2(x, z, x_R; h) = (x - x_R)^2 + (z + h)^2, \tag{2.5}$$

the above kernel can be compactly rewritten as

$$k(x, z, x_T, x_R; h) = \int_{-\infty}^{+\infty} \frac{(x - x_T)(x - x_R) + y^2}{[c^2 + y^2]^{3/2}[p^2 + y^2]^{3/2}}\, \mathrm{d}y.$$

We observe that the integrating function is even in a symmetric domain, therefore, we can compute the integral between 0 and ∞, doubling the result, i.e.,

$$k(x, z, x_T, x_R; h) = 2\int_{0}^{+\infty} \frac{(x - x_T)(x - x_R) + y^2}{[c^2 + y^2]^{3/2}[p^2 + y^2]^{3/2}}\, \mathrm{d}y.$$

To compute the integral above we consider three different cases, in which elliptic integrals of the first and second kinds are involved:

- if $c^2 > p^2$, i.e., $|x - x_T| > |x - x_R|$, then

$$\begin{aligned} &k(x,z, x_T, x_R; h) \\ &\quad = \frac{2}{cp^2(c^2 - p^2)^2} \left[\left[(c^2 + p^2)(x - x_T)(x - x_R) - 2c^2p^2\right] E\left(1 - \frac{p^2}{c^2}\right) \right. \\ &\qquad \left. + p^2 \left[c^2 + p^2 - 2(x - x_T)(x - x_R)\right] K\left(1 - \frac{p^2}{c^2}\right) \right]; \end{aligned}$$

- if $c^2 < p^2$, i.e., $|x - x_T| < |x - x_R|$, then

$$\begin{aligned} &k(x,z, x_T, x_R; h) \\ &\quad = \frac{2}{pc^2(c^2 - p^2)^2} \left[\left[(c^2 + p^2)(x - x_T)(x - x_R) - 2c^2p^2\right] E\left(1 - \frac{c^2}{p^2}\right) \right. \\ &\qquad \left. + c^2 \left[c^2 + p^2 - 2(x - x_T)(x - x_R)\right] K\left(1 - \frac{c^2}{p^2}\right) \right]; \end{aligned}$$

ETNA
Kent State University and
Johann Radon Institute (RICAM)

- if $c^2 = p^2$, then we are computing the electrical conductivity in a point x exactly in the middle between x_T and x_R, i.e., $|x - x_T| = |x - x_R|$. In this case, we have

$$k(x, z, x_T, x_R; h) = \frac{\pi}{8c^5}\left[c^2 + 3(x - x_T)(x - x_R)\right].$$

In the above formulas, $K(q^2)$ denotes the complete elliptic integral of the first kind and $E(q^2)$ the complete elliptic integral of the second kind defined as

$$K(q^2) = \int_0^1 \frac{1}{\sqrt{(1-t^2)(1-q^2t^2)}}\,\mathrm{d}t, \qquad E(q^2) = \int_0^1 \frac{\sqrt{1-q^2t^2}}{\sqrt{1-t^2}}\,\mathrm{d}t, \qquad q^2 < 1.$$

Let us remark that the dependence of the kernel k on z and h comes from the quantities c^2 and p^2 defined in (2.4) and (2.5), respectively.

3. Numerical approximation for the forward model. First of all, we need to solve the forward model to obtain the measurements $g(x_T, x_R; h)$. In applications, we are interested in a limited zone since we cannot take measurements in an unbounded domain. For this reason, we consider the two-dimensional domain $[a, b] \times [0, z_0]$, with $z_0 > 0$; see Figure 2.1. Let us assume that the conductivity vanishes from a certain depth z_0 onward. Therefore, equation (2.3) becomes

$$g(x_T, x_R; h) = \frac{\rho}{\pi}\int_0^{z_0}\int_a^b k(x, z, x_T, x_R; h)\sigma(x, z)\,\mathrm{d}x\,\mathrm{d}z. \tag{3.1}$$

In general, the integral above cannot be computed analytically, so we approximate the integrals appearing in (3.1) by Gauss–Legendre quadrature formulae with n_1 and n_2 nodes, respectively [26]. The Gauss–Legendre quadrature rule is a well-known formula used for approximating the definite integral of a function on the interval $[-1, 1]$, but it can be suitably adapted to our case in the following form

$$\frac{\rho}{\pi}\int_0^{z_0}\int_a^b k(x, z, x_T, x_R; h)\sigma(x, z)\,\mathrm{d}x\,\mathrm{d}z \approx \mathcal{G}_{n_1,n_2},$$

with

$$\mathcal{G}_{n_1,n_2} := \frac{\rho}{\pi}\sum_{i_1=1}^{n_1}\sum_{i_2=1}^{n_2}\lambda_{i_1}\mu_{i_2}k(x_{i_1}, z_{i_2}, x_T, x_R; h)\sigma(x_{i_1}, z_{i_2}),$$

$$\begin{aligned} x_{i_1} &= a + \frac{b-a}{2}(s_{i_1} + 1), & \lambda_{i_1} &= \frac{b-a}{2}w_{i_1}, & i_1 &= 1, \dots, n_1, \\ z_{i_2} &= \frac{z_0}{2}(\widetilde{s}_{i_2} + 1), & \mu_{i_2} &= \frac{z_0}{2}\widetilde{w}_{i_2}, & i_2 &= 1, \dots, n_2, \end{aligned}$$

where $s_{i_1}, \widetilde{s}_{i_2} \in (-1, 1)$ are the zeros of the Legendre orthogonal polynomial in $[-1, 1]$ and w_{i_1}, $\widetilde{w}_{i_2}$ are the corresponding weights for the n_1 and n_2 Gauss–Legendre formula, respectively. This choice of nodes and weights is the only one that allows an m-point quadrature rule to integrate exactly polynomials of degree $2m - 1$.

We report now two different examples to show the effectiveness of the quadrature formula and the accuracy of the approximated electromagnetic data, i.e., the measurements $g(x_T, x_R; h)$. For simplicity, we have considered the same number of nodes in the two variables, i.e., $n_1 = n_2$.

ETNA
Kent State University and
Johann Radon Institute (RICAM)

EXAMPLE 3.1. In this first example, we consider $\sigma(x,z) = e^{(-(0.3(x-4)^2+2(z-1.5)^2))}$ as the function for the conductivity profile. The transmitter and receiver are positioned at $x_T = 2$ and $x_R = 3$, the height at which the measurements are taken is fixed at $h = 1$, and the integration limits are $a = 0$, $b = 10$, and $z_0 = 5$. In this case, we have

$$g(x_T, x_R; h) = \frac{\rho}{\pi} \int_0^5 \int_0^{10} k(x, z, x_T, x_R; h) e^{(-(0.3(x-4)^2+2(z-1.5)^2))} \, \mathrm{d}x \, \mathrm{d}z, \tag{3.2}$$

where the kernel $k(x, z, x_T, x_R; h)$ is defined in Section 2.

As we do not know the exact analytical value of integral (3.2), we consider as the "exact" solution the approximation $\mathcal{G}_{512,512}$. Table 3.1 shows in the second column the results of the approximated integral $\mathcal{G}_{n_1,n_2}$ for different values of $n_1 = n_2$. Moreover, the error $|\mathcal{G}_{512,512} - \mathcal{G}_{n_1,n_2}|$ between the approximation and the "exact" solution is displayed in the last column.

TABLE 3.1
Approximation of $g(x_T, x_R; h)$ for Example 3.1.

$n_1 = n_2$	$\mathcal{G}_{n_1,n_2}$	$\lvert\mathcal{G}_{512,512} - \mathcal{G}_{n_1,n_2}\rvert$
4	0.03856252983724	$4.24 \cdot 10^{-3}$
8	0.03466252927568	$3.45 \cdot 10^{-4}$
16	0.03431463330623	$3.28 \cdot 10^{-6}$
32	0.03431791466368	$1.47 \cdot 10^{-9}$
64	0.03431791613395	$1.05 \cdot 10^{-13}$

As it is expected, by increasing the number of nodes, the error decreases, obtaining an error of order 10^{-13} with $n_1 = n_2 = 64$.

EXAMPLE 3.2. In this example, we consider the same profile for the conductivity, but we change the position of the transmitter and the receiver to $x_T = 4$, $x_R = 5$, and $h = 0.5$. The domain of integration remains the same.

Again, the exact solution $g(x_T, x_R; h)$ is not available, so we consider as "exact" solution the approximation $\mathcal{G}_{512,512}$. From the second and third columns of Table 3.2, we see that, similarly as above, by increasing the number of nodes, the error decreases, obtaining an error of order 10^{-14} with $n_1 = n_2 = 128$.

These results suggest that for any position of the device, the approximation of the right–hand side g is accurate enough to proceed with the inversion procedure.

TABLE 3.2
Approximation of $g(x_T, x_R; h)$ for Example 3.2.

$n_1 = n_2$	$\mathcal{G}_{n_1,n_2}$	$\lvert\mathcal{G}_{512,512} - \mathcal{G}_{n_1,n_2}\rvert$
4	0.08096960456951	$1.04 \cdot 10^{-2}$
8	0.06769701833225	$2.86 \cdot 10^{-3}$
16	0.07000055270036	$5.52 \cdot 10^{-4}$
32	0.07054715911392	$5.56 \cdot 10^{-6}$
64	0.07055271762885	$2.71 \cdot 10^{-9}$
128	0.07055272034261	$2.08 \cdot 10^{-14}$

ETNA
Kent State University and
Johann Radon Institute (RICAM)

4. Inversion algorithm. We now write (3.1) in matrix form. We collocate the equation at the nodes $x_{T_{j_1}} \in [a,b]$ and $x_{R_{j_1}} = x_{T_{j_1}} + \rho$, $h_{j_2} \in [0, h_{\max}]$, with $j_1 = 1, \dots, m_1$ and $j_2 = 1, \dots, m_2$. In this way, our discretized integral equation (3.1) can be written as

$$\frac{\rho}{\pi} \sum_{i_1=1}^{n_1} \sum_{i_2=1}^{n_2} \lambda_{i_1} \mu_{i_2} k(x_{i_1}, z_{i_2}, x_{T_{j_1}}, x_{R_{j_1}}; h_{j_2}) \sigma(x_{i_1}, z_{i_2}) = g(x_{T_{j_1}}, x_{R_{j_1}}; h_{j_2}),$$

and the corresponding linear system of equations can be written as

$$\widehat{M}\sigma = g,$$

where $\widehat{M}$ is a fourth-order tensor with entries

$$(\widehat{M})_{i_1,i_2,j_1,j_2} = \frac{\rho}{\pi} \lambda_{i_1} \mu_{i_2} k(x_{i_1}, z_{i_2}, x_{T_{j_1}}, x_{R_{j_1}}; h_{j_2}),$$

while σ and g are $n_1 \times n_2$ and $m_1 \times m_2$ matrices, respectively, with entries $(\sigma)_{i_1,i_2} = \sigma(x_{i_1}, z_{i_2})$ and $(g)_{j_1,j_2} = g(x_{T_{j_1}}, x_{R_{j_1}}; h_{j_2})$.

To simplify the resolution of the system, we rearrange the matrices and the tensor in lexicographical order obtaining the linear system of equations

$$M\boldsymbol{\sigma} = \mathbf{g}, \tag{4.1}$$

where M is the $m_1 m_2 \times n_1 n_2$ coefficient matrix and $\boldsymbol{\sigma}$ and $\mathbf{g}$ are $n_1 n_2$ and $m_1 m_2$ vectors, respectively.

For simplicity, we consider $N := n_1 = n_2 = m_1$. We vary m_2, that is, the number of heights above the ground at which the measurements are collected. We remark here that, in applications, m_2 is much smaller than N, since the device used for the measurements is hand-used. This means that we will always deal with a very underdetermined system and, consequently, there will exist infinitely many solutions of (4.1).

A solution $\boldsymbol{\sigma}$ of the linear system (4.1) exists only if the right-hand side $\mathbf{g}$ belongs to the range of M. In real applications, the data values are affected by perturbations due to measuring and rounding errors, so one cannot be sure that the perturbed right-hand side lies in the range of M. In other words, the system (4.1) is an ill-posed problem. Therefore, we solve the least-squares minimization problem with a nonnegative constraint on the solution, i.e.,

$$\begin{aligned} &\min_{\boldsymbol{\sigma} \in \mathbb{R}^{n_1 n_2}} \|M\boldsymbol{\sigma} - \mathbf{g}\|^2, \\ &\text{s.t. } \sigma_i \geq 0. \end{aligned}$$

Each component of $\boldsymbol{\sigma}$ has to be nonnegative, since $\boldsymbol{\sigma}$ is the physical quantity that represents the electrical conductivity. Furthermore, the system is very ill-conditioned so it is necessary to introduce a regularization term [24]. In our numerical experiments, we use Tikhonov regularization, that is,

$$\begin{aligned} &\min_{\boldsymbol{\sigma} \in \mathbb{R}^{n_1 n_2}} \|M\boldsymbol{\sigma} - \mathbf{g}\|^2 + \nu \|L\boldsymbol{\sigma}\|^2, \\ &\text{s.t. } \sigma_i \geq 0, \end{aligned} \tag{4.2}$$

where $\nu > 0$ is the regularization parameter and L is a regularization matrix.

Let us remark that a closed form of the solution of the constrained problem (4.2) generally is not available. Many authors have developed different strategies to solve constrained least-squares problems [9, 10]. In this paper, we compute an approximation of the nonnegative

ETNA
Kent State University and
Johann Radon Institute (RICAM)

exact solution in the following way. Let Ω denote the nonnegative cone, and let $\mathcal{P}_\Omega$ be the orthogonal projector from $\mathbb{R}^n$ to Ω. It is trivial to see that $\mathcal{P}_\Omega(\mathbf{x})$, with $\mathbf{x} \in \mathbb{R}^n$, can be computed by setting all negative entries of $\mathbf{x}$ to zero. As an approximation of the nonnegative solution of (4.2) we consider

$$\boldsymbol{\sigma}^\Omega = \mathcal{P}_\Omega((M^T M + \nu L^T L)^{-1} M^T \mathbf{g}),$$

that is, we compute an approximation of the solution by solving the unconstrained Tikhonov problem with a post-projection on the nonnegative cone. The vector $\boldsymbol{\sigma}^\Omega$ generally is a good approximation of $\boldsymbol{\sigma}_{\text{exact}}$, nevertheless there exist other methods to compute accurate approximations of $\boldsymbol{\sigma}_{\text{exact}}$, for example modulus-based iterative methods; see, e.g., [1, 49]. In the following, in order not to burden the notation, we write $\boldsymbol{\sigma}$ in place of $\boldsymbol{\sigma}^\Omega$.

The accuracy of the reconstruction depends on the choice of ν. In our experiments, we consider eight values of $\nu \in [10^{-5}, 5 \cdot 10^{-2}]$, and we pick the parameter between them using two methods. In our first approach, since we deal with synthetic data, we know the exact distribution of the electrical conductivity, so we can select the "best" regularization parameter, that is, the one that minimizes the error between the reconstruction $\boldsymbol{\sigma}_\nu$ and the exact solution $\boldsymbol{\sigma}_{\text{exact}}$

$$\nu_{\text{best}} = \arg\min_\nu \|\boldsymbol{\sigma}_\nu - \boldsymbol{\sigma}_{\text{exact}}\|.$$

We also tested the L-curve criterion [29, 30, 31], since it can be used in real-world scenarios, i.e., when the noise level and the exact solution are unknown. It determines the regularization parameter as the corner, i.e., the point of maximum curvature, of the log-log plot of the (semi)norm $\|L\boldsymbol{\sigma}_\nu\|$ of the regularized solution against the corresponding residual norm $\|M\boldsymbol{\sigma}_\nu - \mathbf{g}\|$, where $\boldsymbol{\sigma}_\nu$ is the approximated solution corresponding to the trial regularization parameter ν.

The matrix L incorporates desirable properties for the solution. It is typically a diagonal weighting matrix (for instance, the identity matrix) or a discrete approximation of a differential operator. For two-dimensional problems, such as in image restoration, one may consider

$$D_{1,\otimes} = \begin{bmatrix} I_{n_2} \otimes D_1 \\ D_1 \otimes I_{n_2} \end{bmatrix} \in \mathbb{R}^{2n_2(n_1-1)\times n_1 n_2},$$

where $\otimes$ denotes the Kronecker product, I_{n_2} is the identity matrix of order n_2, and

$$D_1 = \begin{bmatrix} -1 & 1 & & \\ & \ddots & \ddots & \\ & & -1 & 1 \end{bmatrix} \in \mathbb{R}^{(n_1-1)\times n_1}$$

is an approximation to the first derivative operator.

We remark that the matrix D_1 provides a good regularization operator in one-dimensional problems. If it is used in two-dimensional ones, then numerical experiments show that some artifacts, like vertical lines, appear in the recovered solutions. These are not present when the regularization matrix $D_{1,\otimes}$ is used. This is due to the fact that the latter matrix considers not only the "vertical" direction but also the "horizontal" one.

REMARK 4.1. When we use $L = D_{1,\otimes}$ in the regularization term of equation (4.2), we substitute L by the upper triangular matrix $R \in \mathbb{R}^{n_1 n_2 \times n_1 n_2}$ obtained from the economy-size QR decomposition of L [28], since the orthogonal matrix Q has no effect on the norm.

Finally, in this paper, we perform numerical simulations with synthetic data, that is, we know the exact solution, and the forward model generates the exact measurement datasets $\widehat{\mathbf{g}}$.

ETNA
Kent State University and
Johann Radon Institute (RICAM)

We add to the data a Gaussian noise vector to simulate experimental errors

$$\mathbf{g} = \widehat{\mathbf{g}} + \mathbf{e} = \widehat{\mathbf{g}} + \frac{\varepsilon \|\widehat{\mathbf{g}}\|}{\sqrt{m_1 m_2}} \mathbf{w},$$

where $\mathbf{w}$ is a normally distributed random vector with zero mean and unit variance and ε stands for the noise level.

5. Numerical experiments. In all experiments, we consider the two-dimensional domain $[a, b] \times [0, z_0]$, with $a = 0$, $b = 10$, and $z_0 = 5$. We fix the inter-coil distance $\rho = 1$, which is typical for the EM38 device. Of course, other configurations can be used and give similar results.

All simulations have been performed using MATLAB version 9.15 (R2023b). The most expensive part of the computations is building the tensor $\widehat{M}$, because of the expression of the kernel of the two-dimensional model. The matrices were constructed on an Intel® Xeon® Gold 6136 CPU 3.00GHz processor with 128GB of RAM and 32 cores, running the Ubuntu GNU/Linux operating system. Then, we solve the inverse problem on a laptop computer Intel® Core® i7 CPU 2.80GHz, with 16GB of RAM and 8 cores, running the Debian GNU/Linux operating system.

We consider three different profiles for the conductivity to investigate the performances of the proposed algorithm. We gauge accuracy through the Relative Reconstruction Error

$$\mathrm{RRE}(\boldsymbol{\sigma}) = \frac{\|\boldsymbol{\sigma} - \boldsymbol{\sigma}_{\text{exact}}\|}{\|\boldsymbol{\sigma}_{\text{exact}}\|}.$$

EXAMPLE 5.1. In this first example, we consider the following distribution for the electrical conductivity

$$\sigma(x, z) = e^{-(0.3(x-4)^2 + 2(z-1.5)^2)},$$

that visually corresponds to a sphere with an increasing value of the conductivity towards the center; see Figure 5.1(a). We set $N = 32$ and $m_2 = 5$, with $h_{\max} = 1.3$ meters. In this case, the coefficient matrix M in system (4.1) is a 160×1024 matrix with condition number $\kappa_2(M) \approx 10^{12}$. We first consider a noise level of 10^{-4}, and we use the identity matrix as regularization operator.

In Figure 5.1(a) we report the exact solution, while Figure 5.1(b) and Figure 5.1(c) show the reconstructions obtained with the best regularization parameter, ν_{best}, and the one with the regularization parameter estimated by the L-curve, ν_{cor}, respectively. Both reconstructions are very accurate due to the "small" amount of noise present in the data. The first row of Table 5.1 shows the estimated regularization parameters ν_{best} and ν_{cor} and the RRE for the corresponding regularized solutions. We observe that in both cases we obtain a small error when the large ill-conditioning of the problem is taken into account.

We now compare the application of the standard Tikhonov regularization method with the one with a general regularization term. More precisely, we test as regularization matrices the identity matrix I and $D_{1,\otimes}$. We add a noise level of 10^{-3} to the exact data. Figure 5.2 shows the different reconstructions obtained by the best regularization parameter ν_{best}. To illustrate that $D_{1,\otimes}$ is a very effective regularization operator, we plot in Figure 5.2(c) a single column of the reconstruction, and we compare it with the exact solution. We can see that, even if the value of the maximum is not recovered, we are able to reproduce accurately the shape of the conductivity profile, correctly identifying the depth at which the maximum is placed.

ETNA
Kent State University and
Johann Radon Institute (RICAM)

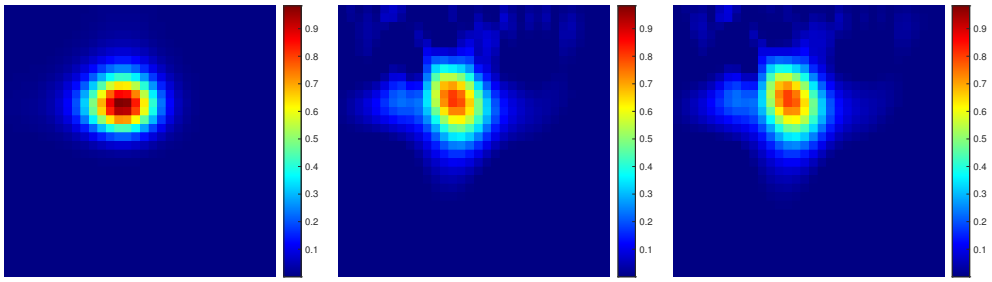

(a) (b) (c)

FIG. 5.1. *Reconstructions of the electrical conductivity for Example 5.1 from data generated by adding a noise level of* 10^{-4}*: the plots show the exact solution (a), the approximate solution corresponding to the best regularization parameter* ν_{best} *(b), and the approximate solution corresponding to the regularization parameter* ν_{cor} *estimate by the L-curve (c).*

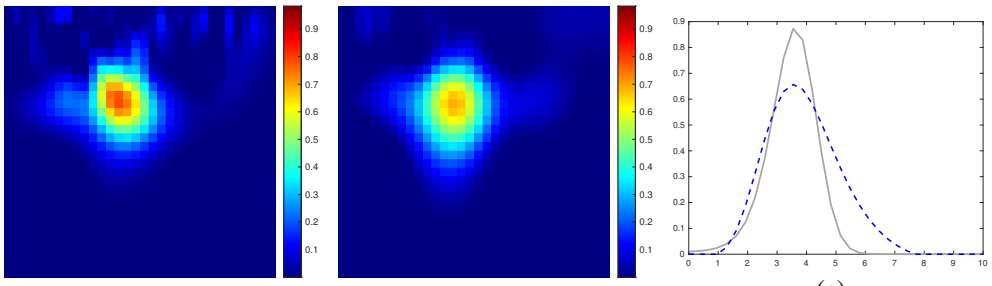

(a) (b) (c)

FIG. 5.2. *Reconstructions of the electrical conductivity for Example 5.1 from data generated by adding a noise level of* 10^{-3}*. The plots show the approximate solution corresponding to the best regularization parameter* ν_{best} *with regularization matrix I (a) and* $D_{1,\otimes}$ *(b). The panel (c) reports the 13-th column of the reconstruction of the electrical conductivity obtained with reg. matrix* $D_{1,\otimes}$ *(blue dashed line) compared to the exact solution (gray solid line).*

We can notice that, in all cases where the algorithm is not able to recover the maximum value of the conductivity, the linear system is strongly underdetermined. Furthermore, the reason for this may also reside in the over-smoothing effect of Tikhonov regularization. However, the results are acceptable enough since we are able to find the position and the shape of the sphere. Improved accuracy often can be achieved by either using non-smooth regularization terms (e.g., ℓ^1-norm [8]) or by employing iterative regularization methods like iterated Tikhonov [7].

EXAMPLE 5.2. We consider the electrical conductivity distribution

$$\sigma(x,z) = e^{-(0.7(x-2.5)^2+2(z-2.5)^2 s} + e^{-(0.7(x-8)^2+3(z-1.5)^2)},$$

which visually corresponds to two spheres; see Figure 5.3(a). We set $N = 64$ and 15 heights for the measurements, i.e., $m_2 = 15$, with $h_{\max} = 1.5$ meters. We first consider a noise level of $\varepsilon = 10^{-4}$, and then we set $\varepsilon = 10^{-3}$. The results for the different noises levels and regularization matrices are reported in Table 5.1.

Figures 5.3(b) and (c) display the best reconstructions, i.e., with ν_{best}, obtained with the regularization matrix $D_{1,\otimes}$ for the two different levels of noise. In this case, the reconstruction of the exact solution is more challenging since we deal with two conductive objects placed

ETNA
Kent State University and
Johann Radon Institute (RICAM)

relatively close. The algorithm is able to find the shape of the spheres and the depth at which they are located, even if the values of the conductivity are not exactly computed.

We recall here that we are solving a linear system of dimensions 960×4096 with a condition number of the order of 10^{16}. We note that this value may be an effect of round-off errors introduced when computing the condition number since the singular values of M decay very quickly to zero. These results illustrate the effectiveness of the algorithm for ill-conditioned and underdetermined problems.

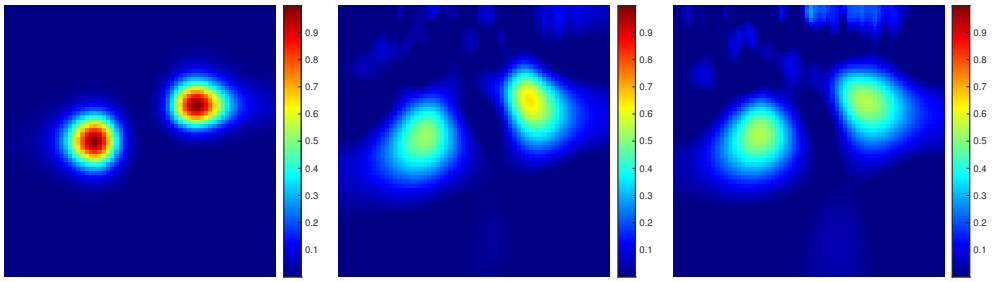

(a) (b) (c)

FIG. 5.3. *Reconstructions of the electrical conductivity for Example 5.2 from data generated by adding a noise level of* 10^{-4} *(b) and* 10^{-3} *(c), compared to the exact solution (a). The regularization matrix is* $D_{1,\otimes}$ *and the regularization parameter is* ν_{best}.

EXAMPLE 5.3. As a last example, we consider a test function for the electrical conductivity that simulates the presence of a layer in the subsoil in which the electrical conductivity is completely different with respect to the environment; see Figure 5.4(a).

As above, we set $N = 64$ and $m_2 = 15$, so the system matrix is the same as the previous example, i.e., the dimensions of M are 960×4096 and its condition number is roughly equal to 10^{16}.

In Figure 5.4(a) we report the exact profile, while the solution obtained with ν_{best} with a noise level of 10^{-3} and regularization matrix I is shown in Figure 5.4(b). Moreover, a plot of a single column of the solution is depicted in Figure 5.4(c).

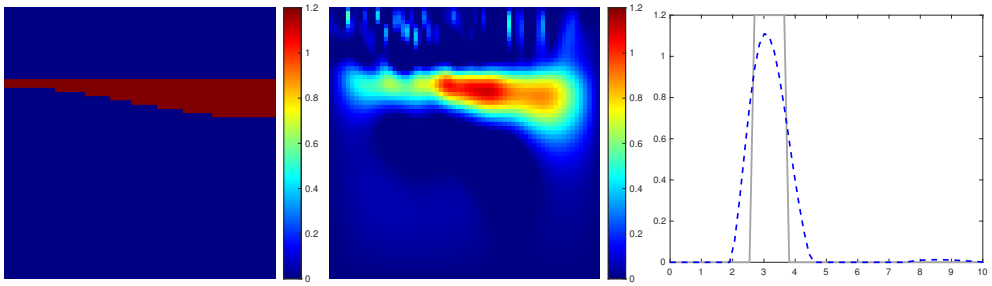

(a) (b) (c)

FIG. 5.4. *Reconstructions of the electrical conductivity for Example 5.3 from data generated by adding a noise level of* 10^{-3} *(b), compared to the exact solution (a). The regularization matrix is* I *and the regularization parameter is* ν_{best}. *Panel (c) reports the reconstruction of the 38-th column (blue dashed line) as well as the exact solution (gray solid line).*

ETNA
Kent State University and
Johann Radon Institute (RICAM)

In Figure 5.4(b) we can observe that the position of the layer in the subsoil is correctly identified. Let us stress that, in this example, we have a nonsmooth single profile of the conductivity; see Figure 5.4(c). We remark that also for nonsmooth variation of the conductivity in the profile of the exact solution, we can obtain acceptable results. In particular, the value of the maximum of the conductivity is almost correctly identified in the center of the layer. For instance, Figure 5.4(c) depicts the 38-th column of the reconstruction compared to the exact step solution.

The RRE for all performed simulations as well as the regularization parameters ν_{best} and ν_{cor} for varying dimensionality, noise level, and regularization matrix, are displayed in Table 5.1.

TABLE 5.1
RRE and regularization parameters ν_{best} and ν_{cor} for Example 5.1, Example 5.2, and Example 5.3.

	N	m_2	ε	L	ν_{best}	$\text{RRE}(\boldsymbol{\sigma}_{\text{best}})$	ν_{cor}	$\text{RRE}(\boldsymbol{\sigma}_{\text{cor}})$
Example 5.1	32	5	10^{-4}	I	$5 \cdot 10^{-5}$	0.2781	$1 \cdot 10^{-4}$	0.2865
	32	5	10^{-3}	I	$1 \cdot 10^{-4}$	0.3067	$5 \cdot 10^{-5}$	0.3596
	32	5	10^{-3}	$D_{1,\otimes}$	$5 \cdot 10^{-4}$	0.3606	$5 \cdot 10^{-3}$	0.4988
Example 5.2	64	15	10^{-4}	I	$1 \cdot 10^{-5}$	0.4653	$5 \cdot 10^{-3}$	0.7369
	64	15	10^{-4}	$D_{1,\otimes}$	$1 \cdot 10^{-5}$	0.4326	$1 \cdot 10^{-4}$	0.6033
	64	15	10^{-3}	I	$5 \cdot 10^{-5}$	0.5907	$5 \cdot 10^{-3}$	0.7370
	64	15	10^{-3}	$D_{1,\otimes}$	$5 \cdot 10^{-5}$	0.4631	$5 \cdot 10^{-3}$	0.9191
Example 5.3	32	15	10^{-3}	I	$1 \cdot 10^{-4}$	0.6308	$1 \cdot 10^{-3}$	0.6973
	32	15	10^{-3}	$D_{1,\otimes}$	$5 \cdot 10^{-4}$	0.6486	$1 \cdot 10^{-2}$	0.7457
	64	15	10^{-3}	I	$5 \cdot 10^{-5}$	0.6314	$5 \cdot 10^{-3}$	0.8107
	64	15	10^{-3}	$D_{1,\otimes}$	$1 \cdot 10^{-4}$	0.6777	$1 \cdot 10^{-3}$	0.6894

6. Conclusions. In this paper we analyzed a two-dimensional model to study the subsoil, mathematically represented by a linear integral equation of the first-kind, which describes the interaction between the soil and an electromagnetic device. A numerical resolution of the forward and inverse problems has been proposed with the aim of reconstructing the electrical conductivity distribution of the subsoil. For the forward model, a Gauss–Legendre quadrature formula for approximating the EM data has been applied. On the other hand, a collocation method, combined with Tikhonov regularization with different regularization matrices and rules for choosing for the regularization parameter, has been employed for the inverse problem. Numerical experiments investigated the performance of the method and confirmed the effectiveness of the whole approach. Extensions to the three-dimensional case and a possible reduction of the computational cost are presently being developed by the authors.

Acknowledgments. The authors thank the anonymous referees for their comments and suggestions which improved the presentation of this paper. The authors are members of the GNCS group of INdAM and are partially supported by INdAM-GNCS 2024 Project "Algebra lineare numerica per problemi di grandi dimensioni: aspetti teorici e applicazioni" (CUP_E53C23001670001). The research of F. Pes is partially supported by Fondazione di Sardegna, Progetto biennale bando 2021, "Computational Methods and Networks in Civil Engineering (COMANCHE)", by INdAM-GNCS 2023 Project "Tecniche numeriche per lo studio dei problemi inversi e l'analisi delle reti complesse" (CUP_E53C22001930001), and she gratefully acknowledges the PRIN 2022 project "Inverse Problems in the Imaging

ETNA
Kent State University and
Johann Radon Institute (RICAM)

Sciences (IPIS)" (2022ANC8HL), OGS and CINECA under HPC-TRES program award number 2024-02. P. Díaz de Alba is partially supported by the INdAM-GNCS 2023 Project "Metodi numerici per modelli descritti mediante operatori differenziali e integrali non locali" (CUP_E53C22001930001) and gratefully acknowledges Fondo Sociale Europeo REACT EU - Programma Operativo Nazionale Ricerca e Innovazione 2014-2020 and Ministero dell'Università e della Ricerca for the financial support.

REFERENCES

[1] Z. Bai, A. Buccini, K. Hayami, L. Reichel, J. Yin, and N. Zheng, *Modulus-based iterative methods for constrained Tikhonov regularization*, J. Comput. Appl. Math., 319 (2017), pp. 1–13.

[2] D. Beamish, *Low induction number, ground conductivity meters: a correction procedure in the absence of magnetic effects*, J. Appl. Geophys., 75 (2011), pp. 244–253.

[3] D. Brenton Myers, N. R. Kitchen, K. A. Sudduth, R. E. Sharp, and R. J. Miles, *Soybean root distribution related to claypan soil properties and apparent soil electrical conductivity*, Crop Sci., 47 (2007), pp. 1498–1509.

[4] A. Buccini and P. Díaz de Alba, *A variational non-linear constrained model for the inversion of FDEM data*, Inverse Problems, 38 (2022), Art. 014001 (21 pages).

[5] A. Buccini, P. Díaz de Alba, and F. Pes, *An alternating direction multiplier method for the inversion of FDEM data*, J. Sci. Comput., 101 (2024), Art. 14 (29 pages).

[6] A. Buccini, P. Díaz de Alba, F. Pes, and L. Reichel, *An efficient implementation of the Gauss–Newton method via generalized Krylov subspaces*, J. Sci. Comput., 97 (2023), Art. 44 (20 pages).

[7] A. Buccini, M. Donatelli, and L. Reichel, *Iterated Tikhonov regularization with a general penalty term*, Numer. Linear Algebra Appl., 24 (2017), Art. e2089 (12 pages).

[8] A. Buccini and L. Reichel, *An ℓ^2-ℓ^q regularization method for large discrete ill-posed problems*, J. Sci. Comput., 78 (2019), pp. 1526–1549.

[9] D. Calvetti, G. Landi, L. Reichel, and F. Sgallari, *Non-negativity and iterative methods for ill-posed problems*, Inverse Problems, 20 (2004), pp. 1747–1758.

[10] D. Calvetti, B. Lewis, L. Reichel, and F. Sgallari, *Tikhonov regularization with nonnegativity constraint*, Electron. Trans. Numer. Anal., 18 (2004), pp. 153–173. https://etna.ricam.oeaw.ac.at/vol.18.2004/pp153-173.dir/pp153-173.pdf

[11] G. P. Deidda, P. Díaz de Alba, C. Fenu, G. Lovicu, and G. Rodriguez, *FDEMtools: a MATLAB package for FDEM data inversion*, Numer. Algorithms, 84 (2020), pp. 1313–1327.

[12] G. P. Deidda, P. Díaz de Alba, F. Pes, and G. Rodriguez, *Forward electromagnetic induction modelling in a multilayered half-space: an open-source software tool*, Remote Sens., 15 (2023), Art. 1772 (36 pages).

[13] G. P. Deidda, P. Díaz de Alba, and G. Rodriguez, *Identifying the magnetic permeability in multi-frequency EM data inversion*, Electron. Trans. Numer. Anal., 47 (2017), pp. 1–17. https://etna.ricam.oeaw.ac.at/vol.47.2017/pp1-17.dir/pp1-17.pdf

[14] G. P. Deidda, P. Díaz de Alba, G. Rodriguez, and G. Vignoli, *Smooth and sparse inversion of EMI data from multi-configuration measurements*, in 2018 IEEE 4th International Forum on Research and Technology for Society and Industry (RTSI) (RTSI 2018), IEEE Conference Proceedings, Los Alamitos, 2018, pp. 213–218.

[15] ———, *Inversion of multiconfiguration complex EMI data with minimum gradient support regularization: a case study*, Math. Geosci., 52 (2020), pp. 945–970.

[16] G. P. Deidda, C. Fenu, and G. Rodriguez, *Regularized solution of a nonlinear problem in electromagnetic sounding*, Inverse Problems, 30 (2014), Art. 125014 (27 pages).

[17] P. Díaz de Alba, L. Fermo, F. Pes, and G. Rodriguez, *Minimal-norm RKHS solution of an integral model in geo-electromagnetism*, in 2021 21st International Conference on Computational Science and Its Applications (ICCSA), IEEE Conference Proceedings, Los Alamitos, 2021, pp. 21–28.

[18] ———, *Regularized minimal-norm solution of an overdetermined system of first kind integral equations*, Numer. Algorithms, 92 (2023), pp. 471–502.

[19] P. Díaz de Alba, L. Fermo, and G. Rodriguez, *Solution of second-kind Fredholm integral equations by means of Gauss and anti-Gauss quadrature rules*, Numer. Math., 146 (2020), pp. 699–728.

[20] P. Díaz de Alba, L. Fermo, C. van der Mee, and G. Rodriguez, *Recovering the electrical conductivity of the soil via a linear integral model*, J. Comput. Appl. Math., 352 (2019), pp. 132–145.

[21] P. Díaz de Alba and G. Rodriguez, *Regularized inversion of multi-frequency EM data in geophysical applications*, in Trends in Differential Equations and Applications, F. Ortegón Gallego, M. Redondo Neble, and J. Rodríguez Galván, eds., SEMA SIMAI Springer Series 8, Springer, Cham, 2016, pp. 357–369.

ETNA
Kent State University and
Johann Radon Institute (RICAM)

[22] J. A. DOOLITTLE, K. A. SUDDUTH, N. R. KITCHEN, AND S. J. INDORANTE, *Estimating depths to claypans using electromagnetic induction methods*, J. Soil Water Conserv., 49 (1994), pp. 572–575.
[23] D. J. DROMMERHAUSEN, D. E. RADCLIFFE, D. E. BRUNE, AND H. D. GUNTER, *Electromagnetic conductivity surveys of dairies for groundwater nitrate*, J. Environ. Qual., 24 (1995), pp. 1083–1091.
[24] H. W. ENGL, M. HANKE, AND A. NEUBAUER, *Regularization of Inverse Problems*, Kluwer, Dordrecht, 1996.
[25] D. V. FITTERMAN, V. F. LABSON ET AL., *Electromagnetic induction methods for environmental problems*, in Near-Surface Geophysics, D. K. Butler, ed., Society of Exploration Geophysicists, Houston, 2012, pp. 301–356.
[26] C. F. GAUSS, *Methodus nova integralium valores per approximationem inveniendi*, Commentationes Societatis Regiae Scientiarum Göttingensis Recentiores, 3 (1814).
[27] M. E. GHARSALLAH, H. AICHI, T. STAMBOULI, Z. BEN RABAH, AND H. BEN HASSINE, *Assessment and mapping of soil salinity using electromagnetic induction and Landsat 8 OLI remote sensing data in an irrigated olive orchard under semi-arid conditions*, Soil Water Res., 17 (2022), pp. 15–28.
[28] G. H. GOLUB AND C. F. VAN LOAN, *Matrix Computations*, 3rd ed., John Hopkins University Press, Baltimore, 1996.
[29] P. C. HANSEN, *Analysis of discrete ill-posed problems by means of the L-curve*, SIAM Rev., 34 (1992), pp. 561–580.
[30] P. C. HANSEN, T. K. JENSEN, AND G. RODRIGUEZ, *An adaptive pruning algorithm for the discrete L-curve criterion*, J. Comput. Appl. Math., 198 (2007), pp. 483–492.
[31] P. C. HANSEN AND D. P. O'LEARY, *The use of the L-curve in the regularization of discrete ill-posed problems*, SIAM J. Sci. Comput., 14 (1993), pp. 1487–1503.
[32] N. R. KITCHEN, K. A. SUDDUTH, AND S. T. DRUMMOND, *Mapping of sand deposition from 1993 midwest floods with electromagnetic induction measurements*, J. Soil Water Conserv., 51 (1996), pp. 336–340.
[33] S. M. LESCH, D. J. STRAUSS, AND J. D. RHOADES, *Spatial prediction of soil salinity using electromagnetic induction techniques: 1. statistical prediction models: a comparison of multiple linear regression and cokriging*, Water Resour. Res., 31 (1995), pp. 373–386.
[34] J. D. MCNEILL, *Electromagnetic terrain conductivity measurement at low induction numbers*, Technical Note TN-6 Geonics Limited, Mississauga, 1980.
[35] ———, *Rapid, accurate mapping of soil salinity by electromagnetic ground conductivity meters*, In Advances in Measurement of Soil Physical Properties: Bringing Theory into Practice, G. C. Topp, W. D. Reynolds, and R. E. Green, eds., Soil Science Society America, SSSA Special Publications 30, 1992, pp. 209–229.
[36] S. MÉNDEZ-DELGADO, E. GÓMEZ-TREVIÑO, AND M. A. PÉREZ-FLORES, *Forward modelling of direct current and low-frequency electromagnetic fields using integral equations*, Geophys. J. Internat., 137 (1999), pp. 336–352.
[37] M. O. OLORUNFEM, M. A. DAN-HASSAN, AND J. S. OJO, *On the scope and limitations of the electromagnetic method in groundwater prospecting in a Precambrian basement terrain—a Nigerian case study*, J. Afr. Earth Sci., 20 (1995), pp. 151–160.
[38] L. PELLERIN, *Applications of electrical and electromagnetic methods for environmental and geotechnical investigations*, Surv. Geophys., 23 (2002), pp. 101–132.
[39] M. A. PÉREZ-FLORES, *Inversión Rápida en 2-D de Datos de Resistividad, Magnetotelúricos y Electromagnéticos de Fuente Controlada a Bajos Números de Inducción*, Ph.D. Thesis, Centro de Investigación Científica y de Educación Superior de Ensenada, México, 1995.
[40] M. A. PÉREZ-FLORES, R. G. ANTONIO-CARPIO, E. GÓMEZ-TREVIÑO, I. FERGUSON, AND S. MÉNDEZ-DELGADO, *Imaging of 3D electromagnetic data at low-induction numbers*, Geophysics, 77 (2012), pp. WB47–WB57.
[41] M. A. PÉREZ-FLORES, S. MÉNDEZ-DELGADO, AND E. GÓMEZ-TREVIÑO, *Imaging low-frequency and DC electromagnetic fields using a simple linear approximation*, Geophysics, 66 (2001), pp. 1067–1081.
[42] F. PES, *Truncated minimal-norm Gauss–Newton method applied to the inversion of FDEM data*, in Computational Science and Its Applications–ICCSA 2023 Workshops, Springer Nature, Cham, 2023, pp. 641–658.
[43] P. A. PETSETIDI AND G. KARGAS, *Assessment and mapping of soil salinity using the EM38 and EM38MK2 sensors: a focus on the modeling approaches*, Land, 12 (2023), Art. 1932 (27 pages).
[44] B. R. SCANLON, J. G. PAINE, AND R. S. GOLDSMITH, *Evaluation of electromagnetic induction as a reconnaissance technique to characterize unsaturated flow in an arid setting*, Groundwater, 37 (1999), pp. 296–304.
[45] B. SIEMON, A. V. CHRISTIANSEN, AND E. AUKEN, *A review of helicopter-borne electromagnetic methods for groundwater exploration*, Near Surf. Geophys., 7 (2009), pp. 629–646.
[46] K. A. SUDDUTH, S. T. DRUMMOND, AND N. R. KITCHEN, *Accuracy issues in electromagnetic induction sensing of soil electrical conductivity for precision agriculture*, Comput. Electron. Agric., 31 (2001), pp. 239–264.
[47] K. A. SUDDUTH, N. R. KITCHEN, D. BRENTON MYERS, AND S. T. DRUMMOND, *Mapping depth to argillic soil horizons using apparent electrical conductivity*, J. Environ. Eng. Geophys., 15 (2010), pp. 135–146.

ETNA
Kent State University and
Johann Radon Institute (RICAM)

[48] F. VISCONTI AND J. M. DE PAZ, *Sensitivity of soil electromagnetic induction measurements to salinity, water content, clay, organic matter and bulk density*, Precis. Agric., 22 (2021), pp. 1559–1577.
[49] N. ZHENG, K. HAYAMI, AND J.-F. YIN, *Modulus-type inner outer iteration methods for nonnegative constrained least squares problems*, SIAM J. Matrix Anal. Appl., 37 (2016), pp. 1250–1278.